Chinese Chemical Letters 36 (2025) 109746

Contents lists available at ScienceDirect

Chinese Chemical Letters

journal homepage: www.elsevier.com/locate/cclet

Mixed-charge glycopolypeptides as antibacterial coatings with long-term activity

Fangping Yang[1], Jin Shi[1], Yuansong Wei, Qing Gao, Jingrui Shen, Lichen Yin, Haoyu Tang*

Institute of Functional Nano & Soft Materials (FUNSOM), Collaborative Innovation Center of Suzhou Nano Science and Technology, Soochow University, Suzhou 215123, China

ARTICLE INFO

Article history:
Received 10 January 2024
Revised 29 February 2024
Accepted 5 March 2024
Available online 8 March 2024

Keywords:
Antibacterial coating
Glycopolypeptide
Bactericidal activity
Fouling
Biofilm

ABSTRACT

Planktonic bacteria adhere and subsequently form biofilms on implantable medical devices can cause severe infections that have become the major types of hospital-acquired infections. Traditional coatings for the implants are frequently lack of long-term antifouling and bactericidal activities. It is still a big challenge to simultaneously improve the antifouling and bactericidal activities of the coatings. Herein, we report that mixed-charge glycopolypeptide coatings are of long-term antibacterial activities to efficiently inhibit the biofilm growth. The glycosylation of mixed-charge polypeptides has led to a significant improvement of both antifouling and bactericidal activities. The cooperative effect of the saccharide residues and mixed-charge residues improved the resistance of the polypeptide coatings against protein adsorption. The saccharide and L-glutamic acid (E) residues collectively enhanced the bacterial membrane-disruption of cationic L-lysine (K) residues, leading to potent bactericidal activity. Meanwhile, the glycopolypeptide coatings showed superior biocompatibility, long-term antibiofilm and anti-infection properties in two types of mouse subcutaneous infection models and one type of mouse urinary tract infection model. This work provides a new strategy to achieve antibacterial coatings with long-term activities for preventing implantable medical device associated infections.

With the improvement of medical technique, various implantable medical devices (*e.g.*, catheters and prosthetics) have been developed and widely used to help repair tissue, restore biological functions, and so on [1]. Meanwhile, implant surfaces have provided a "comfortable" platform for bacteria adhesion and subsequent biofilm formation, which has led to high rate of device-associated infections (DAIs) [2,3]. While planktonic bacteria can be readily killed by anbiotics and other anibacterial agents [4] such as antimicrobial peptides (AMPs) [5,6] and silver nanoparticles [7,8], they are able to adhere and subsequently form biofilms on implantable medical devices, causing severe infections. Biofilms are difficult to eliminate, frequently causing the removal and secondary implantation of the medical devices. Therefore, strategies that can prevent biofilm formation are highly desirable to combat DAIs. Antibacterial coatings with antifouling or bactericidal activities have exhibited short-term (less than two weeks) inhibition of biofilm formation [9,10]. However, antifouling coatings are not able to kill bacteria [11,12]. Eventually, bacteria can conquer the hydration layer of an antifouling coating by bacterial pilus and adhesins, leading to bacterial adhesion and biofilm formation. While bactericidal coatings can kill bacteria by contact or by releasing antibiotics [13], reactive oxygen species (ROS) [14] or AMPs [15]. The surface bactericidal activity was frequently screened by dead bacteria [16]. Moreover, bactericidal coatings, such as cationic polymer coatings have raised biocompatibility issues, which need to be further addressed.

Therefore, antibacterial coatings with both antifouling and bactericidal activities have been developed to address the DAI issues [17,18]. Generally, they are composed of both hydrophilic (*e.g.*, hydroxyl groups and poly(ethylene glycol) (PEG)) and bactericidal (*e.g.*, cationic groups and AMPs) components to achieve antifouling and bactericidal activities, respectively [19,20]. The two distinct functional components can be randomly or separately integrated in a polymer. Much effort has been made to pursue potent surface antibacterial properties by adjusting the chemical structures and compositions of the functional groups. Nevertheless, different functional components are frequently lack of cooperative effect, consequently leading to inadequate antibacterial activity. For example, mixed-charge polypeptide coatings with equivalent L-lysine (K) and L-glutamic acid (E) residues displayed resistance to both

* Corresponding author.
E-mail address: hytang@suda.edu.cn (H. Tang).
[1] These authors contributed equally to this work.

https://doi.org/10.1016/j.cclet.2024.109746
1001-8417/

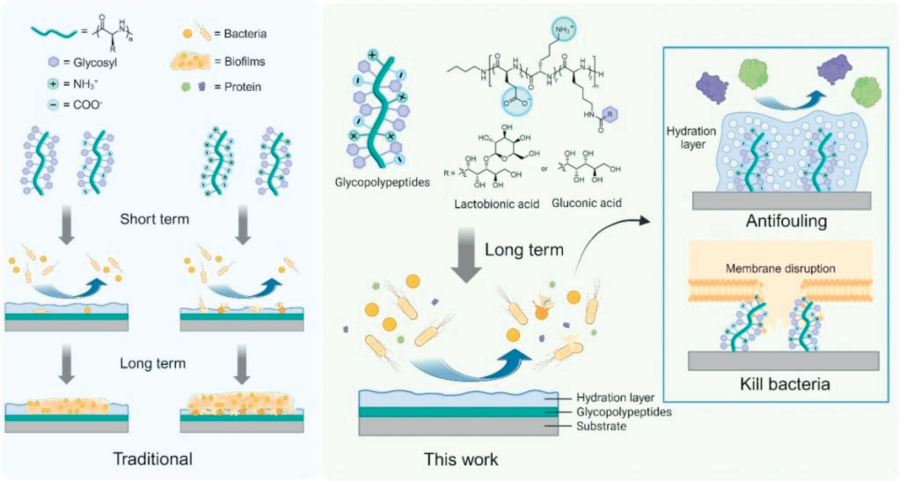

Fig. 1. Schematic illustration of the mixed-charge glycopolypeptide coatings and their long-term antibacterial activities originating from simultaneously improved antifouling and bactericidal activities.

protein adsorption and bacterial adhesion due to the hydration of hydrophilic groups, including carboxyl ($-COO^-$) and ammonium ($-NH_3^+$) groups [21–23]. Yet, they displayed lower bactericidal activity than cationic polypeptide or AMP coatings owing to the electronic interactions between K and E residues, which weakened the membrane-disruption of cationic groups. In order to potentiate the surface antibacterial property, the exploration and discovery of functional components that can simultaneously improve the antifouling and bactericidal activities are of great importance.

In nature, carbohydrates play unique roles in biological functions. For instance, the glycocalyx of cells is a carbohydrate-rich layer composed of glycosylated proteins, lipids, and so on [24]. Carbohydrates of the glycocalyx are engaged in cell recognition and cell-cell interactions [25]. Inspired by the structure and function of glycocalyx, researchers have designed the glycosylated AMPs and cationic polymers that have shown improved targeting specificity in solution [26]. The glycosylated surfaces have showed switchable bacterial adhesion by tuning the carbohydrate-protein (*i.e.*, FimH lectin) interactions [27] or fouling resistance ascribing to the hydration of carbohydrates and steric hindrance effect [28]. However, glycosylated surfaces with potent antifouling and bactericidal activities have not been developed.

Herein, we report the design, synthesis, and biological properties of a new series of glycopolypeptides (*i.e.*, $E_{xn}K_{pn}K_{qn}$(Glu) or $E_{xn}K_{pn}K_{qn}$(Lac)) composed of three distinct functional components, including E, K, and saccharide-conjugated K residues (Fig. 1). The glycopolypeptides were deposited on implant surfaces with the assistance of polydopamine (PDA) forming potent antibacterial coatings. The structure-property relationship of the glycopolypeptide coatings was systematically investigated. The surface antibacterial mechanisms were revealed by a series of experiments that indicated a cooperative effect of different functional components. For the first time, we discovered that the saccharide residues can improve both antifouling and bactericidal activity of the mixed-charge polymer coatings. The top-performing glycopolypeptide coating displayed biocompatibility and long-term (*i.e.*, 28 days) antibacterial activity both *in vitro* and *in vivo*.

The glycopolypeptides were synthesized by ring-opening polymerizations (ROPs) of α-amino-acid-based *N*-carboxyanhydrides (NCAs) and side-chain modifications (Fig. 2A and Scheme S1 in Supporting information). N_ε–*tert*-butyloxycarbonyl-L-lysine NCA (BLL-NCA) and γ-benzyl-L-glutamate NCA (BLG-NCA) were used as the monomers to yield E and K residues, respectively. The NCAs were initiated by *n*-butylamine and the ROPs were performed in anhydrous DMF at room temperature. The monomer conversion was monitored by Fourier transform-infrared (FTIR) spectroscopy. The resulting polypeptides (*i.e.*, BK_{yn} and $BE_{xn}BK_{yn}$) were precipitated in cold diethyl ether when the $\nu_{C=O}$ band of NCA rings at 1853 cm^{-1} in the FTIR spectra completely disappeared. The degree of polymerization (DP) was controlled by adjusting the initial molar ratio of the monomer and initiator (*i.e.*, $[M]_0/[I]_0$). The numbers of E and K residues (*i.e.*, x_n and y_n) in a single polypeptide chain were tuned by changing the feeding ratio of BLL-NCA and BLG-NCA. The number-average molecular weight (M_n) and molecular weight dispersity ($Đ$) were determined by gel permeation chromatography (GPC) equipped with a multi-angle laser light scattering (MALLS) detector. The GPC determined M_ns are close to the theoretical ones and the $Đ$s are relatively small ($\leq$1.19), suggesting that the *n*-butylamine initiated ROPs of BLL-NCA and BLG-NCA are well-controlled (Fig. S1 and Tables S1 and S2 in Supporting information).

The molecular structures of BK_{yn} and $BE_{xn}BK_{yn}$ were confirmed by ^{1}H nuclear magnetic resonance (^{1}H NMR) spectroscopy (Fig. 2B and ^{1}H NMR spectra section in Supporting information). For example, the chemical shifts at 5.06 and 3.81 ppm correspond to the protons of the benzyl methylene of E residues and ε-carbon of K residues, respectively. Therefore, the E/K ratios can be determined by ^{1}H NMR based on the integration ratios of the above protons. They are close to the feeding ratios further indicating the well-controlled ROPs. Moreover, the DPs were determined by the ^{1}H NMR according to the integration ratios of the protons of the benzyl methylene of E residues, ε-carbon of K residues and methyl end groups.

BK_{yn} and $BE_{xn}BK_{yn}$ underwent deprotection of *tert*–butyloxycarbonyl (Boc) and benzyl groups under acidic conditions, yielding the polypeptides with amino pendants (*i.e.*, K_{yn} and $E_{xn}K_{yn}$, Fig. 2A and Scheme S1). A mixed-charge polypeptide, namely $E_{15}K_{15}$ was synthesized. It has been reported that the balance of E and K residues in the mixed-charge polypeptide coatings are important to achieve potent surface antibacterial property [18]. The glycosylation of K_{yn} and $E_{xn}K_{yn}$ *via* the amidation reaction yielded the designed glycopolypeptides (*i.e.*, $E_{xn}K_{pn}K_{qn}$(Glu) and $E_{xn}K_{pn}K_{qn}$(Lac)) with mixed-charge pendants. Gluconic acid and lactobionic acid were used for the glycosylation. Because that they are commercially available in a large scale and composed of 5 or 8 nonionic and highly hydrophilic hydroxyl groups. The mixed-charge glycopolypeptides with constant numbers of E and K residues and different number of saccharide residues

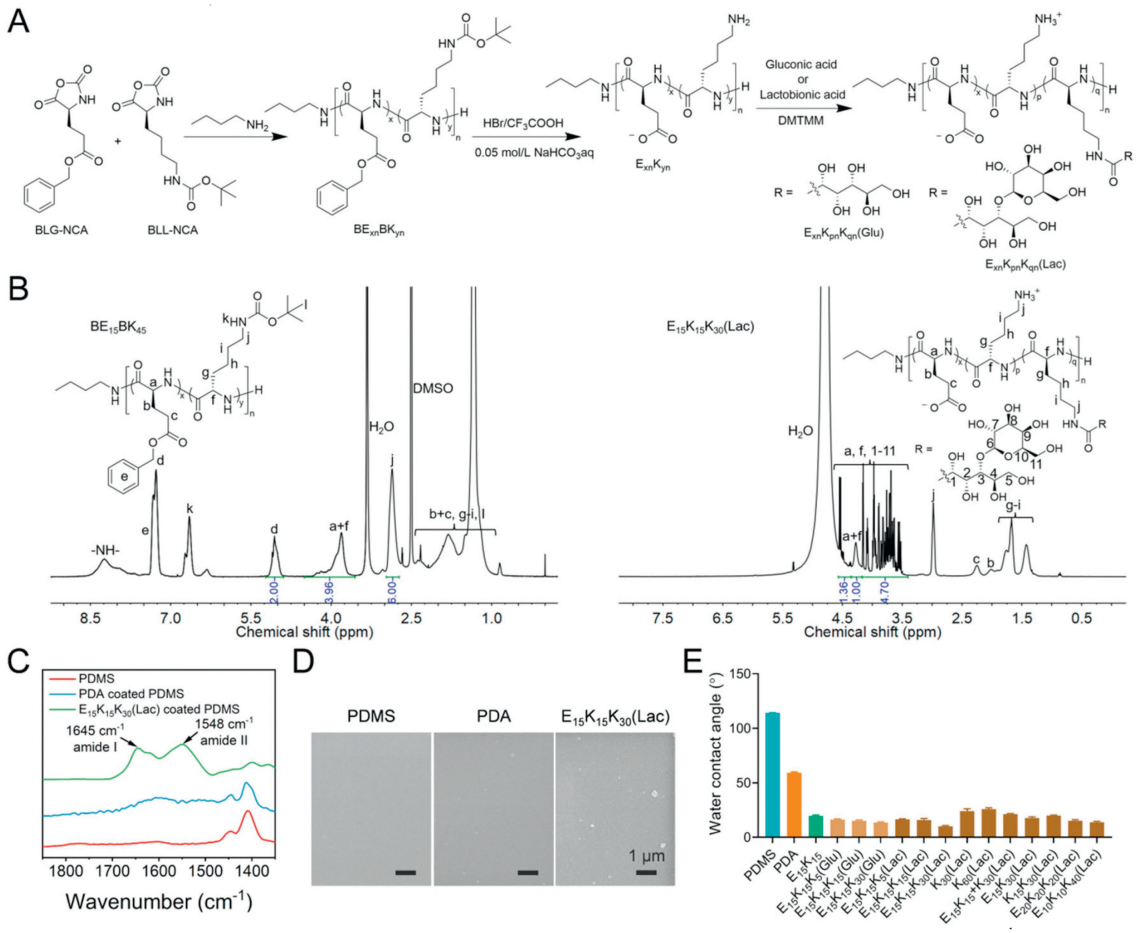

Fig. 2. (A) Synthetic routes of the mixed-charge glycopolypeptides, namely $E_{xn}K_{pn}K_{qn}$(Glu) and $E_{xn}K_{pn}K_{qn}$(Lac). (B) ^{1}H NMR spectra of $BE_{15}BK_{45}$ in DMSO–d_6 and $E_{15}K_{15}K_{30}$(Lac) in D_2O. (C) FTIR spectra and (D) SEM images of the uncoated, PDA, and $E_{15}K_{15}K_{30}$(Lac) coated PDMS. Scale bar: 1 μm. (E) Water contact angles of the uncoated, PDA, $E_{15}K_{15}$, glycopolypeptides coated PDMS. Data are mean ± standard deviation (SD) (n = 3).

($E_{15}K_{15}K_{qn}$(Glu) and $E_{15}K_{15}K_{qn}$(Lac), qn = 5, 15, and 30) were synthesized. However, their DPs are different. In order to further investigate the effect of the content of saccharide residues on the biological properties, $E_{20}K_{20}K_{20}$(Lac) and $E_{10}K_{10}K_{40}$(Lac) with the same DP were synthesized. The glycopolypeptides with exclusive lactose (K_{30}(Lac) and K_{60}(Lac)), E/lactose ($E_{15}K_{30}$(Lac)) or K/lactose ($K_{15}K_{30}$(Lac)) residues were also synthesized to compare with the mixed-charge glycopolypeptides, aiming to explore the role of the charge groups on the biological properties.

The molecular structures of the $E_{15}K_{15}$ and all resulting glycopolypeptides were also confirmed by ^{1}H NMR (Fig. 2B and ^{1}H NMR spectra section in Supporting information). For example, the chemical shifts at 3.56–4.59 ppm correspond to the protons of lactose. The missing chemical shifts at 5.01 and 1.35 ppm suggest successful deprotection of both benzyl and Boc groups with high conversions.

All resulting polypeptides can be readily dissolved in aqueous solutions, such as Tris–HCl buffer (pH 8.5), enabling their coating preparation from a safe and environmental-friendly solution. Prior to the coating preparation, we investigated the polypeptide conformation and polymer surface charges in aqueous solutions by circular dichroism (CD) spectroscopy and dynamic light scattering (DLS) technique. The solution conformations of the $E_{15}K_{15}$, K_{30}(Lac), K_{60}(Lac), $E_{15}K_{30}$(Lac), and $K_{15}K_{30}$(Lac) in pH range of 4.5–9.5 are random-coils (Fig. S2 in Supporting information), indicating that the charge repulsion or steric hindrance effect disrupt intermolecular hydrogen bonds of α-helix. The mixed-charge glycopolypeptides also adopt random-coil conformations at pH 7.4. However, $E_{15}K_{15}K_5$(Glu), $E_{15}K_{15}K_5$(Lac) under low pH conditions (*e.g.*, pH 5.5), and $E_{15}K_{15}K_{30}$(Glu), $E_{15}K_{15}K_{30}$(Lac) under high pH conditions (*e.g.*, pH 8.5) adopt small portion of α-helical conformation as evidence that the mean residue ellipticity at 222 nm, $[\theta]_{222}$ increased at specific pH values. The pH-induced coil-to-helix conformation transition usually involves the protonation of amino pendants or deprotonation of carboxyl pendants. Yet, the mixed-charge glycopolypeptides adopt different solution conformations under the same pH conditions. The structure-conformation relationship is still unclear. Moreover, the zeta potential analysis of $E_{15}K_{15}$ and all mixed-charge glycopolypeptides revealed a zero zeta potential under the neutral condition (Fig. S3 in Supporting information), suggesting an equal amount of negative and positive charges, namely carboxyl ($-COO^-$) and ammonium ($-NH_3^+$) group.

Polydimethysiloxane (PDMS), namely silicone was used as the substrate. It has been widely used in implantable medical devices owing to its desirable elasticity, good chemical stability, and biocompatibility [11,29]. The polypeptide coatings on PDMS slides were prepared *via* a codeposition process in the dopamine (DA) Tris–HCl buffer solution (pH 8.5). It can self-polymerize in weak basic solution with the presence of oxidative reagents, such as oxygen, depositing and forming a PDA coating on various substrates [30]. The chemical interactions between PDA and low polarity polymer substrate (*e.g.*, poly(tetrafluoroethylene) and PDMS) are mainly van der Waals and hydrophobic interactions [31]. The PDA coatings can be readily used as an adhesion layer for further surface modifications. Water-soluble polymers can be readily de-

posited on various substrates with the assistance of DA [32]. The codeposition process usually involves the self-polymerization of DA, Michael addition reactions, hydrogen bonding interactions, and so on [33]. The chemical interactions between polymer coatings and PDA coatings are mainly hydrogen bonding, cationic-π, and π-π interactions [33]. Previous evidence has indicated that polymer coatings prepared by DA-assisted codeposition process are of good stability against soaking in various aqueous solutions, ultrasonication, and autoclaving [32,34]. The mixed-charge glycopolypeptides, such as $E_{15}K_{15}K_{30}$(Lac) self-assembled in Tris–HCl buffer solution (pH 8.5) forming nanoscale aggregates mainly owing to the intermolecular electrostatic interactions (Fig. S4 in Supporting information). Similar results were observed in the polymer/DA solutions. The addition of DA increased the hydrodynamic diameters of polymers, suggesting the presence of interactions (*e.g.*, electrostatic interactions and hydrogen bonds) between the glycopolypeptides and DA molecules.

Besides the polypeptide coatings, we also prepared PEG and melittin coatings to compare their surface biological properties. PEG is widely used for antifouling applications [35]. Melittin is a commercially available AMP and has high surface bactericidal activity by contact [34,36]. Polymer blend coatings, namely $E_{15}K_{15}/K_{30}$(Lac) and melittin/PEG_{227} coatings were also prepared to investigate the effect of functional component distribution (blend or random copolymer) on the surface biological properties.

All polymer coatings were successfully prepared as confirmed by a combination of characterization techniques, including FTIR, X-ray photoelectron spectroscopy (XPS), and scanning electron microscopy (SEM). In the FTIR spectra of polypeptide, melittin, and polymer blend coatings (Fig. 2C and Fig. S5 in Supporting information), the appearance of characteristic amide I and amide II bands corresponding to the peptide bonds suggests the formation of polymer coatings on PDMS surfaces. In addition, the FTIR band at 1466 cm^{-1} corresponds to the bending vibration of $–CH_2–$, verifying the preparation of PEG_{227} coating. In the XPS spectra, uncoated PDMS showed O 1s, C 1s, Si 2s, and Si 2p peaks at 532.0, 284.5, 99.0, and 154.0 eV, respectively (Fig. S6 in Supporting information). After deposition of PDA on the PDMS surface, a characteristic N 1s peak appeared in the XPS spectrum of PDA coating. While all polypeptides and melittin coatings are of the N 1s peak in the XPS, their N 1s binding energy were different from PDA coating. Polypeptides are composed of peptide bonds whereas PDA contains indole moieties. Moreover, PEG_{227} coated PDMS did not show the N 1s peak in the XPS because of the small amount of DA used in codeposition process (polymer to DA weight ratio was 16/1) and weak N 1s peak of PDA layer covered by PEG_{227}.

The surface morphologies of the polymer coatings were characterized by SEM. The unmodified PDMS surface was flat without any noticeable nanoscale structures (Fig. 2D and Fig. S7 in Supporting information). PDA coating showed slightly increased roughness and few nanoparticles randomly distributed on the surface, likely due to the poorly controlled self-polymerization of DA. The polymer coatings prepared from polypeptides, melittin, PEG_{227}, and polymer blends are of rougher surface morphologies than both PDMS and PDA coating (Fig. 2D and Fig. S7). The thickness of the polymer coatings in the dry state was measured by spectroscopic ellipsometry (Fig. S8 in Supporting information). $E_{15}K_{15}$, glycopolypeptides, PEG_{227}, melittin and polymer blend coatings. The thickness of $E_{15}K_{15}$, glycopolypeptides, PEG_{227}, melittin, and polymer blend coatings was in the range of 200–360 nm. Given that all polymer coatings were non-leachable, we reasoned that the coating thickness should not affect the surface biological properties, including antifouling, bactericidal, and biocompatible properties.

The water contact angles of the unmodified PDMS and the polymer coatings were measured by a drop shape analysis instrument. The unmodified PDMS surface was highly hydrophobic with a contact angle of 110.7° whereas the PDA coating was hydrophilic (59.2°, Fig. 2E). All polypeptide coatings are highly hydrophilic with water contact angles below 27.2°, ascribing to their large amounts of hydrophilic pendants, such as carboxyl ($-COO^-$), ammonium ($-NH_3^+$), and saccharide groups. Glycosylation of polypeptides resulted in increased hydrophilicity as evidence that $E_{15}K_{15}K_{qn}$(Glu) and $E_{15}K_{15}K_{qn}$(Lac) showed lower water contact angles than $E_{15}K_{15}$. Moreover, $E_{15}K_{15}K_{30}$(Lac) showed lower water contact angles than $E_{15}K_{15}$, K_{30}(Lac), and $E_{15}K_{15}/K_{30}$(Lac), suggesting a cooperative effect of the charges and saccharides that enhanced the hydration of the random copolymer coatings.

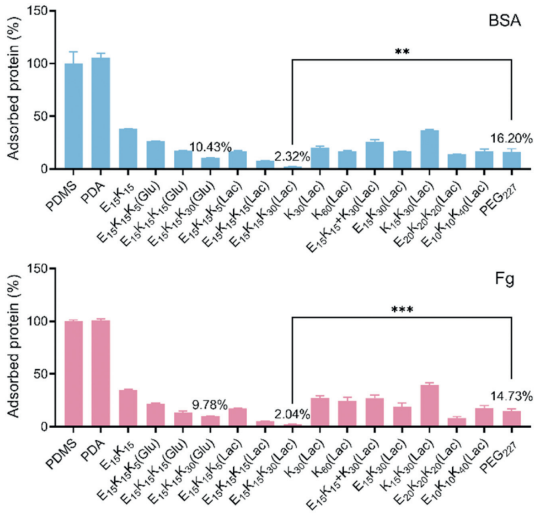

Fig. 3. Adsorbed protein (%) on the uncoated, PDA, $E_{15}K_{15}$, glycopolypeptides, PEG_{227}, and polymer blend coated PDMS surfaces. Data are mean ± SD (n = 3). $^{**}P < 0.01$, $^{***}P < 0.001$.

Protein adsorption resistance of the unmodified PDMS and the polymer coatings was measured by the micro-BCA assay (Fig. S9 in Supporting information). Bovine serum albumin (BSA) and fibrinogen (Fg) were chosen as the model proteins because that they are important proteins in blood and frequently related to bacterial adhesion on material surfaces [37]. The adsorbed proteins on uncoated PDMS surfaces were defined as 100%. High protein adsorption resistance is usually related to potent antifouling property of polymer coatings [38,39]. Both uncoated and PDA coated surfaces showed poor resistance against protein adsorption (Fig. 3). In comparison, the protein adsorption on all polypeptide coatings (<39.4%) was significantly lower than uncoated PDMS surface, ascribing to the formation of hydration layers around the hydrophilic polypeptides that are able to inhibit non-specific protein adsorption and initial bacterial adhesion. The trend of resistance of each polymer against BSA and Fg adsorption was similar. For example, the adsorbed BSA or Fg were 20.8% and 28.3% on K_{30}(Lac) coating, respectively.

Glycosylation of mixed-charge polypeptides (*e.g.*, $E_{15}K_{15}$) resulted in enhanced resistance against protein adsorption. The adsorbed protein decreased with the increase of saccharide residues for the $E_{15}K_{15}K_{qn}$(Glu) and $E_{15}K_{15}K_{qn}$(Lac) coatings. Nevertheless, $E_{15}K_{15}K_{30}$(Lac) coating with 50% saccharide residues showed lower protein adsorption resistance than both $E_{20}K_{20}K_{20}$(Lac) (33% saccharide residues) and $E_{10}K_{10}K_{40}$(Lac) (67% saccharide residues) coatings, suggesting that the protein adsorption resistance was collectively affected by the content of saccharide residues and DP. The mixed-charge glycopolypeptides with lactose pendants showed lower protein adsorption resistance than the ones with glucose pendants, presumably due to the increased hydrogen bonds between lactose pendants and water.

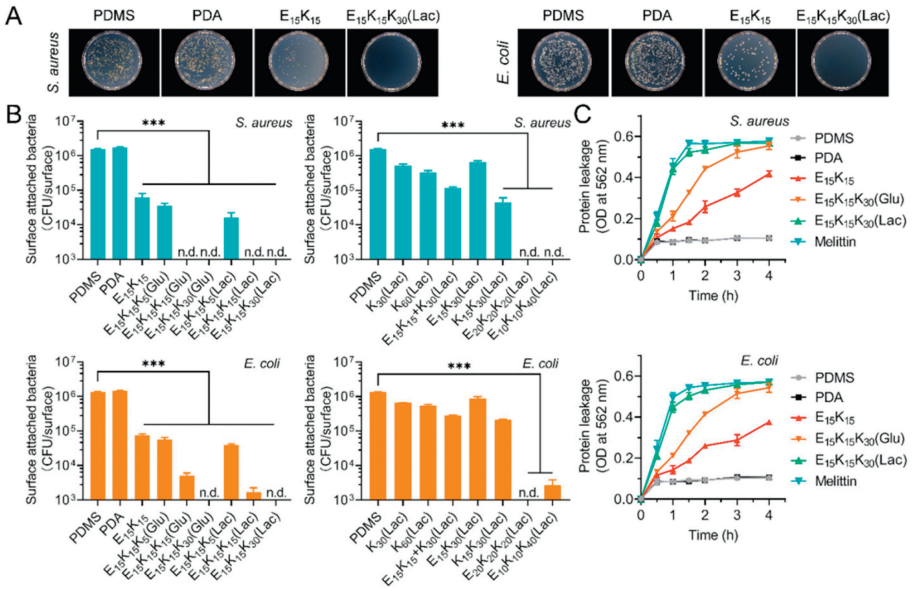

Fig. 4. (A) Representative images of the LB agar plates treated with *S. aureus* and *E. coli* from uncoated and different polymer coated surfaces. (B) Statistical data of colony count of surviving bacteria from the uncoated, PDA, $E_{15}K_{15}$, glycopolypeptides, PEG_{227}, melittin, and polymer blend coated PDMS. (C) Plots of protein leakage *versus* time for the uncoated, PDA, $E_{15}K_{15}$, $E_{15}K_{15}K_{30}$(Glu), $E_{15}K_{15}K_{30}$(Lac), and melittin coated PDMS. Data are mean ± SD ($n = 3$). $^{***}P < 0.001$.

$E_{15}K_{15}K_{30}$(Lac) coating showed significant lower protein adsorption resistance than $E_{15}K_{15}$, K_{30}(Lac), and $E_{15}K_{15}/K_{30}$(Lac), indicating the cooperative effect of the charges and saccharides that enhanced the polymer-water interactions. Increasing the DP of K_{qn}(Lac) slightly enhanced the resistance against protein adsorption. The balance of negative and positive charges played an important role on the resistance against protein adsorption. Specifically, $E_{15}K_{15}K_{30}$(Lac) coating showed significant lower protein adsorption resistance than $E_{15}K_{30}$(Lac) and $K_{15}K_{30}$(Lac), respectively. Moreover, the protein adsorption resistance of $E_{15}K_{15}K_{30}$(Lac) coating was much lower than PEG_{227} coating. As compared to other developed antifouling coatings, $E_{15}K_{15}K_{30}$(Lac) coating showed higher protein adsorption resistance than tetra(ethylene glycol)-based single-chain cyclized/knotted polymer coatings [40], PEG-based single-chain nanoparticle coatings [41], and anionic polymer coatings [42].

The bactericidal activities of the polymer coatings were investigated by a contact-killing assay. *S. aureus* and *E. coli* were used as the model bacteria. They are widely used Gram-positive (*i.e.*, *S. aureus*) and Gram-negative bacteria (*i.e.*, *E. coli*) for surface antibacterial property evaluation. *S. aureus* is usually associated with the infections of skin, bloodstream, and bones while *E. coli* often cause the urinary tract infections [43]. In the contact-killing assay, the bacterial suspension solution was added to coating surfaces which were subsequently covered by a pristine polyethylene (PE) membrane and incubated at 37 °C for 24 h. Then, the surviving bacteria on the polymer coatings were counted by an agar plate colony counting assay (Fig. 4A). The uncoated PDMS, PDA and PEG_{227} coatings showed no bactericidal activity against *S. aureus* or *E. coli*. K_{qn}(Lac) and $E_{15}K_{30}$(Lac) coatings showed insignificant bactericidal activities whereas the polymer coatings prepared from $E_{15}K_{15}$, mixed-charge glycopolypeptides, and $K_{15}K_{30}$(Lac) showed more than 1.5 log-reduction of *S. aureus* and 1.3 log-reduction of *E. coli* as compared to the uncoated PDMS.

It was interesting to observe that the glycosylation of mixed-charge polypeptides resulted in significantly improved bactericidal activities, especially for the samples with 15–40 residues of saccharides. For example, $E_{15}K_{15}K_{30}$(Glu), $E_{15}K_{15}K_{30}$(Lac), and $E_{20}K_{20}K_{20}$(Lac) coatings showed >99.9% bactericidal efficiency against both *S. aureus* and *E. coli*. The bactericidal kinetic results indicated that $E_{15}K_{15}$ coating only killed 73.1% *S. aureus* and 67.8% *E. coli* after incubation for 4 h whereas $E_{15}K_{15}K_{30}$(Glu) and $E_{15}K_{15}K_{30}$(Lac) coatings killed more than 95.3% bacteria by contact, indicating the importance of glycosylation to enhance the bactericidal activities (Fig. S10 in Supporting information). $E_{15}K_{15}K_{30}$(Lac) coating showed similar bactericidal efficiency (>99.9%) and killing rate to the AMP (melittin) coating. As compared to other developed bactericidal coatings, $E_{15}K_{15}K_{30}$(Lac) coating showed higher bactericidal efficiency than positively charged quaternary ammonium and hydrophobic benzyl group modified poly(lysine methacrylamide) coatings [44] and imidazolium-based polymer coatings [16].

The bactericidal efficiencies of the mixed-charge glycopolypeptide coatings are related to the saccharide structures and contents, and polymer chain length. The polymer coatings with lactose residues showed higher bactericidal activities than the coatings with glucose residues (Fig. 4B). $E_{15}K_{15}K_{30}$(Lac) coating also showed higher killing rate than $E_{15}K_{15}K_{30}$(Glu) coating (Fig. S10).

For the $E_{15}K_{15}K_{qn}$(Glu) and $E_{15}K_{15}K_{qn}$(Lac) coatings, the bactericidal efficiency increased with the increase of saccharide residue contents (from 14% to 50%). $E_{10}K_{10}K_{40}$(Lac) coating with 67% saccharide residues showed slightly lower bactericidal efficiency than $E_{15}K_{15}K_{30}$(Lac) coating. For the coatings with the same saccharide residues, $E_{20}K_{20}K_{20}$(Lac) coating with long polymer chains showed higher bactericidal efficiency than $E_{15}K_{15}K_{15}$(Lac) coating.

Another interesting observation is that the mixed-charge glycopolypeptide coatings showed significantly enhanced bactericidal activities than the cationic glycopolypeptide coating. For example, $E_{15}K_{15}K_{30}$(Lac) coating showed >99.9% bactericidal efficiency whereas $K_{15}K_{30}$(Lac) coating showed 97.8% against *S. aureus* and 82.5% against *E. coli*. This phenomenon indicates that the E residues are essential functional components to potentiate the bactericidal activities probably by improving the polymer-bacterium interactions.

Moreover, $E_{15}K_{15}K_{30}$(Lac) showed higher bactericidal efficiency than $E_{15}K_{15}/K_{30}$(Lac) coating, indicating that the bactericidal activities cannot be improved by simply blending polymers. The polymer blend coatings, including melittin/PEG_{227} and $E_{15}K_{15}/K_{30}$(Lac) coatings showed significantly decreased bactericidal activities as compared to melittin and $E_{15}K_{15}$ coatings.

The surface bactericidal mechanism of the polymer coatings was first investigated by SEM. The uncoated and polymer coated PDMS slides were incubated with *S. aureus* or *E. coli* at 37 °C for 24 h. Loosely adhered bacteria were gently washed off by phosphate buffer saline (PBS) buffer. The morphologies of attached bacteria on polymer surfaces were observed by SEM (Fig. S11 in Supporting information). The bacteria on uncoated and PDA coated surfaces are of regular shapes (spherical or columnar). In comparison, the bacteria shrank on the mixed-charge glycopolypeptide coatings, eventually forming severely deformed cells or cell membranes. Similar results were observed on $E_{15}K_{15}$ and melittin coatings. We speculated that the bactericidal mechanism of the resulting polypeptide coatings was a membrane disruption mechanism [45]. To further verify this mechanism, the protein leakage assay was used to analyze the bacterial membrane damage after contacting with different surfaces. The protein leakages from uncoated and PDA coated surfaces were not noticeable whereas the leakage from melittin coating was fast and significant (Fig. 4C), owing to the electrostatic interaction between melittin and bacterial membranes. It is known that the melittin-bacterium interactions can induce pores in membranes and increase membrane permeability [46,47]. Noticeable protein leakages were observed for the $E_{15}K_{15}$ and mixed-charge glycopolypeptide coatings. In particular, the protein leakage rate from $E_{15}K_{15}K_{30}$(Lac) coating was similar to the melittin coating. We speculated that the $E_{15}K_{15}$ and mixed-charge glycopolypeptide coatings are of the same bactericidal mechanism as the melittin coatings, namely the electrostatic interaction between the cationic residues (*e.g.*, K) and anionic bacterial membranes.

Glycosylation improved the surface bactericidal activities, presumably ascribing to the enhanced polymer-bacterium interactions. To verify this assumption, we modified the polymers with rhodamine B and observed the polymer treated bacteria under the confocal laser scanning microscope (CLSM). $E_{15}K_{15}$ treated bacteria showed no fluorescence whereas both $E_{15}K_{15}K_{30}$(Glu) and $E_{15}K_{15}K_{30}$(Lac) treated bacteria showed intense blue fluorescence (Fig. S12 in Supporting information), owing to the accumulation of $E_{15}K_{15}K_{30}$(Glu) and $E_{15}K_{15}K_{30}$(Lac) on the bacterial surfaces. These results confirmed that the saccharide residues could enhance polymer-bacterium interactions. Moreover, both $E_{15}K_{15}K_{30}$(Glu) and $E_{15}K_{15}K_{30}$(Lac) showed bactericidal activities in solution as evidence that the bacterial membranes were disrupted and aggregated.

Besides the saccharide residues, E and K residues also played important roles on the polymer-bacterium interactions and surface bactericidal activities. To this end, we analyzed the binding affinity between the polymer coatings and bacterial surface proteins that related to the initial bacterial adhesion. Staphylococcal protein A (SpA) was used as the model protein from bacterial surfaces because of its biological function to initiate *S. aureus* adhesion to the abiotic substrates [48]. The binding constant (K_a) of K_{30}(Lac)-SpA was close to K_{60}(Lac)-SpA (Fig. S13 and Table S3 in Supporting information), indicating negligible effect of DP on the binding affinity. The K_a of $E_{15}K_{15}K_{30}$(Lac)-SpA was about two times higher than that of $E_{15}K_{15}$-SpA. It was also 1.4 and 4.7 times higher than those of $K_{15}K_{30}$(Lac)-SpA and $E_{15}K_{30}$(Lac)-SpA, respectively. These results indicated that the saccharide, E, and K residues collectively affected the polymer-bacterium interactions.

The antibiofilm property of the polymer coatings was evaluated by soaking the PDMS slides in bacterial suspension solutions and incubating for 2–28 days. The surface attached bacteria were counted by the agar plate colony counting assay (Figs. S14 and S15 in Supporting information). The biofilm growth was defined as the percentage of surface attached bacteria on polymer coatings as compared to those on the uncoated PDMS surface (Fig. 5A). After incubation for 48 h, the uncoated and PDA coated surfaces were covered by the *S. aureus* or *E. coli* biofilms, due to their poor antibiofilm property. The K_{30}(Lac), K_{60}(Lac), $E_{15}K_{30}$(Lac), and PEG_{227} coatings showed good antibiofilm property, owing to the formation of hydration layers around the hydrophilic polymer chains that inhibited the initial bacterial adhesion. The *S. aureus* biofilm growth on K_{30}(Lac) and K_{60}(Lac) coatings was faster than the *E. coli* biofilm growth, likely resulting from the different saccharide-bacterium interactions. While the biofilm growth on the PEG_{227} coating was low ($\leq$1.18%) after 48 h, the biofilm will eventually form because the PEG_{227} coating has no bactericidal activity. While the melittin coating has potent bactericidal activity by contact, the biofilm can readily grow on dead bacteria attached to the melittin coating leading to fast biofilm growth ($\geq$43.50%). The melittin/PEG_{227} coating showed faster biofilm growth than the PEG_{227} coating, suggesting that the melittin component suppressed the antifouling property of PEG_{227} component.

The biofilm growth on the $E_{15}K_{15}$ coating was faster than the PEG_{227} coating, but slower than the melittin coating. The glycosylation of the mixed-charge polypeptide has achieved extremely low biofilm growth. The $E_{15}K_{15}K_{30}$(Lac) coating showed near zero biofilm growth ($\leq$0.06%) after 48 h, indicating superior antibiofilm property. We speculate that the good antibiofilm property of glycopolypeptide coating is related to the simultaneously improved antifouling and bactericidal activities. Specifically, the hydration layer formation of the polypeptide coatings can inhibit the initial bacterial adhesion. Once the bacteria conquer the hydration layer by bacterial pilus and interact with the polypeptides, they can be readily killed by the membrane disruption mechanism.

We further investigated the antibiofilm property of the $E_{15}K_{15}K_{30}$(Lac) coating for potential long-term uses. The adhered bacteria and biofilms on the material surfaces were observed by CLSM (Fig. 5B). After 3 days incubation, thick and dense biofilms were formed on the uncoated PDMS slides. In comparison, zero biofilm was attached to the $E_{15}K_{15}K_{30}$(Lac) coating even after 28 days incubation, indicating a long-term antibacterial activity. Moreover, the ultralow biofilm formation on the glycopolypeptide coatings after 28 days incubation further indicated good durability of the coatings, because that the biofilm can easily formed on PDMS surfaces within 48 h if the glycopolypeptide coatings were damaged or degraded. The agar plate colony counting assay was used to quantify the biofilm growth (Fig. 5C and Fig. S15). The biofilm growth on the $E_{15}K_{15}K_{30}$(Lac) coating was extremely slow that it was 0.27% for *S. aureus* and 0.78% for *E. coli* after 28 days. So far, polymer coatings with long-term antibacterial activities have been rarely discovered. The antibiofilm property of $E_{15}K_{15}K_{30}$(Lac) coating after 28 days were similar to the ultrahigh molecular weight poly(*N*,*N*-dimethyl acrylamide) coating [32] and poly(3-sulfopropyl methacrylate-*co*-3-acrylamidopropyl trimethylammonium chloride) coating [49].

The hemolysis of the polymer coatings was measured by soaking the polymer coated PDMS slides in the red blood cell (RBC) suspension solution for 1 h, followed by analysis the optical densities (OD) of the supernatants of the RBC suspension solution treated by the polymer coatings and the controls. The RBCs in PBS and Triton X-100 solution (1% in PBS, v/v) were used as the negative and positive controls, respectively.

The uncoated, PDA, and PEG_{227} coated PDMS surfaces showed negligible hemolysis (<0.1%, Fig. S16 in Supporting information). However, the melittin coating lysed 92.4% RBCs within an hour, indicating high cytotoxicity. The melittin/PEG_{227} coating also showed high hemolysis (92.3%), suggesting that the PEG_{227} component cannot suppress the membrane disruption of the melittin component. All polypeptide coatings showed extremely low hemolysis (<2.0%), indicating low toxicity toward the RBCs. The glycosylation of $E_{15}K_{15}$ decreased the hemolysis likely owing to the improved antifouling property by incorporation of saccharide residues.

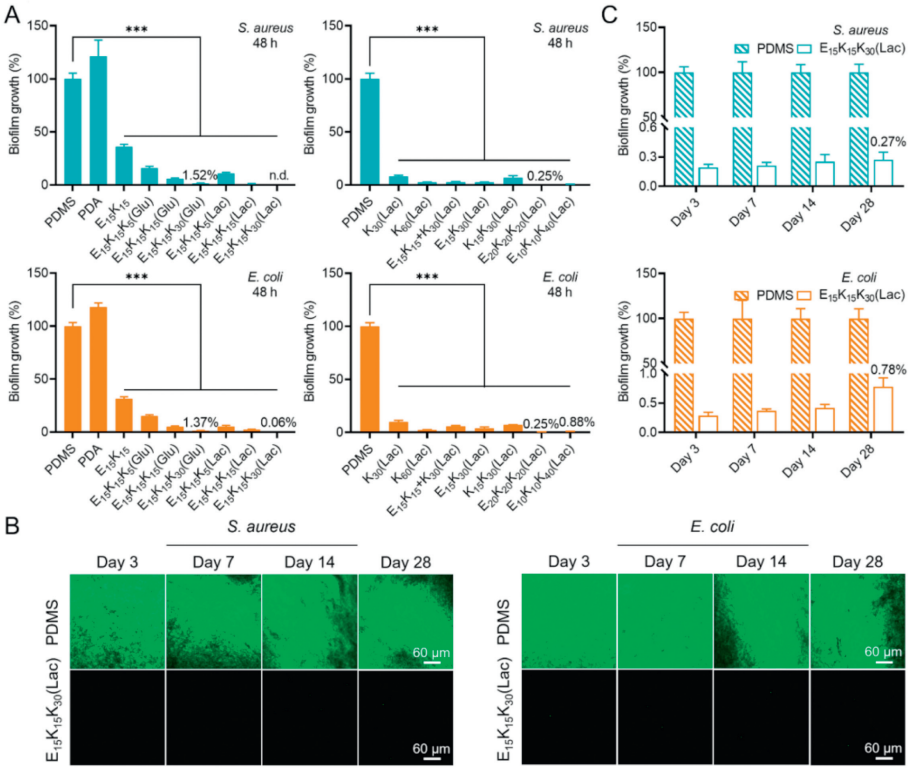

Fig. 5. (A) Biofilm growth on the uncoated, PDA, $E_{15}K_{15}$, glycopolypeptides, PEG_{227}, melittin, and polymer blend coated PDMS after culturing for 48 h ($n = 3$). ***$P < 0.001$. n.d., signifies not detected. (B) CLSM images of *S. aureus* and *E. coli* after culturing for 3–28 days on the uncoated and $E_{15}K_{15}K_{30}$(Lac) coated PDMS. The bacteria were stained with a mixture of SYTO 9 (green: live and dead) and PI (red: dead) solution (in dark, 20 min). Scale bar: 60 μm. (C) Biofilm growth on the uncoated and $E_{15}K_{15}K_{30}$(Lac) coated PDMS after culturing for 3–28 days. Data are mean ± SD ($n = 3$).

The cytotoxicity of the polymer coatings was evaluated by gently covering the polymer coated PDMS slides on the mammalian cells, incubating for 24 h, and measuring the cell viability by a MTT assay. HEK 293T renal epithelial cells and NIH 3T3 fibroblast cells were used as the model cells. Similar to the hemolysis results that the uncoated, PDA, and PEG_{227} coated PDMS surfaces showed negligible cytotoxicity toward the mammalian cells, but the melittin and melittin/PEG_{227} coatings killed near all the cells by contact (Fig. S17 in Supporting information). All polypeptide coatings showed high cell viability, indicating negligible cytotoxicity. For example, the glycosylation of $E_{15}K_{15}$ decreased the hemolysis. For example, the cell viability of NIH 3T3 cell covered by the $E_{15}K_{15}$, K_{30}(Lac), and $E_{15}K_{15}K_{30}$(Lac) coatings were >98%, suggesting that the mixed-charge and saccharide residues cannot disrupt the mammalian cell membranes. In comparison, the cationic glycopolypeptide [$K_{15}K_{30}$(Lac)] coating showed slightly decreased cell viability of both HEK 293T cells and NIH 3T3 cells due to the positively charged polymer chains that can destabilize the cell membranes.

Moreover, the *in vivo* biocompatibility of the $E_{15}K_{15}K_{30}$(Lac) coated PDMS slide was evaluated by a mouse subcutaneous implantation model. The animal experiments were approved by the Institutional Animal Care and Use Committee at Soochow University. The animal experimental protocols were performed by the NIH guidelines for the care and use of laboratory animals (NIH Publication No. 85–23 Rev. 1985). After implantation for 14 days (Fig. S18A in Supporting information), the implant surrounding tissues were evaluated by the histological analysis (Fig. S18B in Supporting information). The tissues were not damaged or diseased that no obvious inflammatory reaction was observed, indicating good *in vivo* biocompatibility of the $E_{15}K_{15}K_{30}$(Lac) coating.

The $E_{15}K_{15}K_{30}$(Lac) coating was used to explore the *in vivo* anti-infection property of the mixed-charge glycopolypeptides. To this end, we established two types of mouse subcutaneous infection models against *S. aureus* and one type of mouse urinary tract infection model against *E. coli*. *S. aureus* and *E. coli* were used in the *in vivo* experiments because that they are known to cause skin and urinary tract infections, respectively. In the subcutaneous infection models, the $E_{15}K_{15}K_{30}$(Lac) coated PDMS slides were treated by *S. aureus* before or after implantation to simulate the bacterium contaminated implants prior to or after the surgery. The uncoated PDMS slide was used as the control. After implantation for 14 days, the skin above the uncoated PDMS implant became red and swollen (Fig. 6A and Fig. S19A in Supporting information) owing to the severe bacterial infection. In comparison, the skin above the $E_{15}K_{15}K_{30}$(Lac) coated PDMS implant has self-healed after 14 days. The agar plate colony counting assay was used to quantify the implant surface attached *S. aureus* (Fig. 6B and Fig. S19B in Supporting information). More than 3.0 log reduction of *S. aureus* was observed for the $E_{15}K_{15}K_{30}$(Lac) coated PDMS implant after 3 days (Fig. 6C and Fig. S19C in Supporting information), suggesting the potent *in vivo* anti-infection property. The implant surrounding tissues were evaluated by the histological analysis on days 3, 7, and 14 (Fig. 6D and Fig. S19D in Supporting information). Large number of inflammatory cells was observed in the subcutaneous tissue contacted with the uncoated PDMS implant. In comparison, no obvious inflammatory reaction was observed in the subcutaneous tissue contacted with the $E_{15}K_{15}K_{30}$(Lac) coated PDMS implant.

In the mouse urinary tract infection model, the urinary catheter was inserted into the mouse urethra and bladder, followed by injection of *E. coli* into the bladder *via* a syringe. The agar plate colony counting assay and the histological analysis were performed

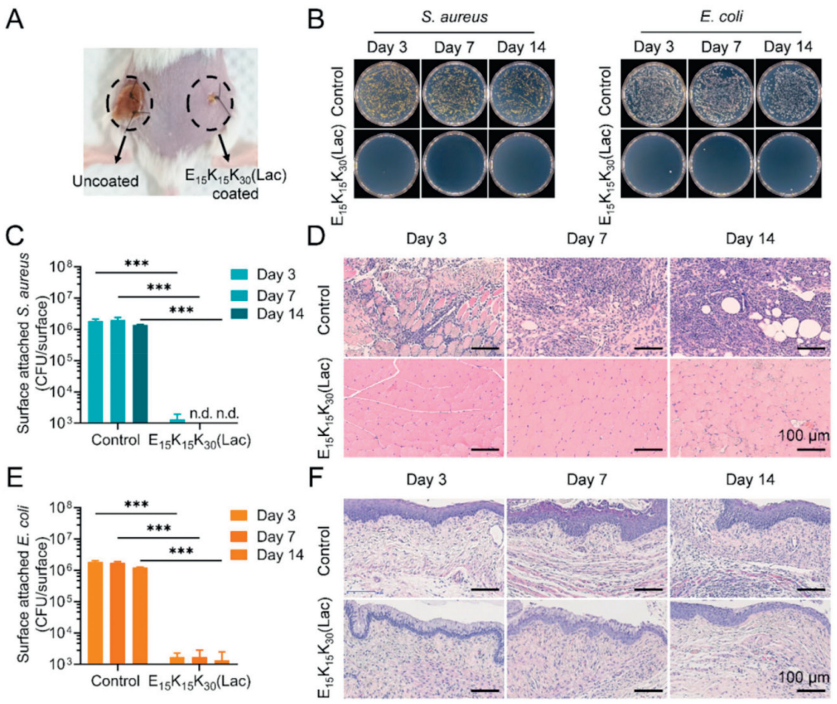

Fig. 6. (A) Picture of the mouse's back implanted by uncoated (left) and $E_{15}K_{15}K_{30}$(Lac) (right) coated PDMS slides after incubation with *S. aureus* on day 14. *S. aureus* suspension solution was injected into the incisions after implantation. (B) Representative images of the LB agar plates treated with detached the *S. aureus* from the uncoated (control) and $E_{15}K_{15}K_{30}$(Lac) coated PDMS slides or the *E. coli* from the uncoated (control) and $E_{15}K_{15}K_{30}$(Lac) coated urinary catheters after implantation for 3, 7, and 14 days. (C) Statistical data of colony count of surviving bacteria from the uncoated (control) and $E_{15}K_{15}K_{30}$(Lac) coated PDMS slides. (D) Hematoxylin and eosin (H&E) staining images of the uncoated (control) and $E_{15}K_{15}K_{30}$(Lac) coated PDMS surrounding subcutaneous tissues after implantation for 3, 7, and 14 days. (E) Statistical data of colony count of surviving bacteria from the uncoated (control) and $E_{15}K_{15}K_{30}$(Lac) coated urinary catheters. (F) H&E staining images of the uncoated (control) and $E_{15}K_{15}K_{30}$(Lac) coated urinary catheter surrounding urethral tissues after implantation for 3, 7, and 14 days. Data are mean ± SD ($n = 3$). $^{***}P < 0.001$. Scale bar: 100 μm.

on days 3, 7, and 14 (Figs. 6B and E). The *E. coli* colonies detached from the uncoated and $E_{15}K_{15}K_{30}$(Lac) coated urinary catheters on day 3 were 1.60×10^6 and 1.20×10^3 CFU/mL, respectively (Fig. 6E), indicating that the $E_{15}K_{15}K_{30}$(Lac) coating inhibited >99.9% biofilm growth. After 14 days of implantation, the uncoated urinary catheter was blocked by the biofilm whereas no noticeable biofilm formation was observed on the $E_{15}K_{15}K_{30}$(Lac) coated urinary catheter. The histological analysis indicated large number of inflammatory cells in the uncoated urinary catheter surrounding urethral tissues from day 3 to day 14 (Fig. 6F), whereas the tissues around the $E_{15}K_{15}K_{30}$(Lac) coated urinary catheters showed insignificant inflammation reaction even on day 14.

In summary, we demonstrate the first example of mixed-charge glycopolypeptide coatings with long-term antibacterial activities and good biocompatibility. The cooperative hydration effect of the saccharide residues and mixed-charge residues enables higher resistance against BSA or Fg adsorption than the coatings prepared from the mixed-charge polypeptide, glycopolypeptide with exclusive saccharide residues, and polypeptide blends. Both saccharide and L-glutamic acid residues play essential roles on the enhancement of the membrane-disruption of cationic residues. Consequently, the mixed-charge glycopolypeptide coatings showed superior antibiofilm properties due to the simultaneously improved antifouling and bactericidal activities. The top-performing coating, namely $E_{15}K_{15}K_{30}$(Lac) coating showed extremely low protein adsorption, outperformed traditional antifouling polymer (PEG_{227}) coating. It also showed high bactericidal efficiency against both *S. aureus* and *E. coli* (>99.9%), and fast killing rate similar to the traditional AMP (melittin) coating. *In vitro* biofilm growth on the $E_{15}K_{15}K_{30}$(Lac) coating was near zero during a short-term period (*e.g.*, 0–2 days) and less than 0.8% during a long-term period (*e.g.*, 3–28 days). All mixed-charge glycopolypeptide coatings showed negligible hemolysis and cytotoxicity. The $E_{15}K_{15}K_{30}$(Lac) coating showed potent *in vivo* bactericidal activity to prevent subcutaneous implant associated infections. It also showed *in vivo* long-term antibiofilm property to significantly inhibit the urinary catheter associated infection. The mixed-charge glycopolypeptides can be readily used as antibacterial coatings on various implantable medical devices (such as urinary catheters, prostheses, implantable healthcare dressings, and so on) to prevent biofilm formation and infection in long-term.

Declaration of competing interest

The authors declare that they have no known competing financial interests or personal relationships that could have appeared to influence the work reported in this paper.

Acknowledgments

We acknowledge the financial support from the National Natural Science Foundation of China (No. 51873213), Science and Technology Program of Suzhou (No. SKY2022111), Collaborative Innovation Center of Suzhou Nano Science & Technology, and FUNSOM Self-Directed Research Project (No. 2022). Jin Shi thanks Biorender.com for the assistance of drawing of graphic abstract and Fig. 1.

Supplementary materials

Supplementary material associated with this article can be found, in the online version, at doi:10.1016/j.cclet.2024.109746.

References

[1] H.J. Busscher, H.C. van der Mei, G. Subbiahdoss, et al., Sci. Transl. Med. 4 (2012) 153rv110.
[2] C.R. Arciola, D. Campoccia, L. Montanaro, Nat. Rev. Microbiol. 16 (2018) 397–409.
[3] S.S. Magill, J.R. Edwards, W. Bamberg, et al., New Engl. J. Med. 370 (2014) 1198–1208.
[4] X. Wang, M. Zhang, T. Zhu, et al., Adv. Sci. 10 (2023) 2206154.
[5] D. Wei, X. Zhang, Biosaf. Health 4 (2022) 118–134.
[6] J. Ding, H. Xiao, X. Chen, Biosaf. Health 4 (2022) 59–60.
[7] Z. Geng, Z. Cao, J. Liu, Exploration 3 (2023) 20210117.
[8] G. Liu, Y. Zhou, Z. Xu, et al., Chin. Chem. Lett. 34 (2023) 107705.
[9] X. Ding, S. Duan, X. Ding, et al., Adv. Func. Mater. 28 (2018) 1802140.
[10] X. Chu, F. Yang, H. Tang, Chin. J. Chem. 40 (2022) 2988–3000.
[11] B. McVerry, A. Polasko, E. Rao, et al., Adv. Mater. 34 (2022) 2200254.
[12] B.B. Berking, G. Poulladofonou, D. Karagrigoriou, et al., Angew. Chem. Int. Ed. 62 (2023) e202308971.
[13] E.M. Hetrick, M.H. Schoenfisch, Chem. Soc. Rev. 35 (2006) 780–789.
[14] L. Cheng, B. Zhou, M. Qi, et al., Chin. Chem. Lett. 35 (2024) 108648.
[15] M. Kazemzadeh-Narbat, H. Cheng, R. Chabok, et al., Crit. Rev. Biotechnol. 41 (2021) 94–120.
[16] R. Xue, X. Chu, F. Yang, et al., ACS Macro Lett. 11 (2022) 387–393.
[17] X. Wang, M. Shan, S. Zhang, et al., Adv. Sci. 9 (2022) 2104843.
[18] R. Yang, X. Wang, S. Yan, et al., Prog. Polym. Sci. 118 (2021) 101409.
[19] L. Mi, S. Jiang, Angew. Chem. Int. Ed. 53 (2014) 1746–1754.
[20] X. Laloyaux, E. Fautre, T. Blin, et al., Adv. Mater. 22 (2010) 5024–5028.
[21] S. Chen, Z. Cao, S. Jiang, Biomaterials 30 (2009) 5892–5896.
[22] X. Chu, F. Wu, Z. Liu, et al., ACS Macro Lett. 12 (2023) 428–432.
[23] Z. Liu, F. Yang, W. Si, et al., ACS Macro Lett. 11 (2022) 1373–1377.
[24] S. Munro, Trends Cell Biol. 10 (2000) 552–553.
[25] C. Reily, T.J. Stewart, M.B. Renfrow, J. Novak, Nat. Rev. Nephrol. 15 (2019) 346–366.
[26] N.G. Bednarska, B.W. Wren, S.J. Willcocks, Drug Discov. Today 22 (2017) 919–926.
[27] T. Weber, V. Chandrasekaran, I. Stamer, et al., Angew. Chem. Int. Ed. 53 (2014) 14583–14586.
[28] H.O. Ham, S.H. Park, J.W. Kurutz, et al., J. Am. Chem. Soc. 135 (2013) 13015–13022.
[29] M. Lam, V. Migonney, C. Falentin-Daudre, Acta Biomater. 121 (2021) 68–88.
[30] H. Lee, S.M. Dellatore, W.M. Miller, P.B. Messersmith, Science 318 (2007) 426.
[31] L. Xie, X. Cui, J. Liu, et al., ACS Appl. Mater. Interfaces 13 (2021) 6941–6950.
[32] Y. Mei, K. Yu, J.C.Y. Lo, et al., ACS Nano 12 (2018) 11881–11891.
[33] H.A. Lee, E. Park, H. Lee, Adv. Mater. 32 (2020) 1907505.
[34] F. Yang, H. Liu, Y. Wei, et al., Acta Biomater. 155 (2023) 359–369.
[35] F.J. Xu, Chin. Chem. Lett. 30 (2019) 2051–2052.
[36] M. Zhu, P. Liu, Z.W. Niu, et al., Chin. Chem. Lett. 28 (2017) 703–708.
[37] J.M. Patti, B.L. Allen, M.J. McGavin, et al., Annu. Rev. Microbiol. 48 (1994) 585–617.
[38] Z. Song, R. Li, X. Yang, A. Ambrosi, X. Luo, Chin. Chem. Lett. 34 (2023) 108314.
[39] X. Hu, J. Tian, C. Li, et al., Adv. Mater. 32 (2020) 2000128.
[40] Q. Xu, S. A, M. Venet, et al., Angew. Chem. Int. Ed. 58 (2019) 10616–10620.
[41] X. Tian, R. Xue, F. Yang, et al., Biomacromolecules 22 (2021) 4306–4315.
[42] R. Xue, X. Zhang, Y. Wei, et al., Biomater. Sci. 9 (2021) 6425–6433.
[43] J.H. Ch'ng, K.K.L. Chong, L.N. Lam, et al., Nat. Rev. Microbiol. 17 (2019) 82–94.
[44] J. Lv, J. Jin, J. Chen, et al., ACS Appl. Mater. Interfaces 11 (2019) 25556–25568.
[45] D. Liu, Y. Xi, S. Yu, et al., Biomaterials 293 (2023) 121957.
[46] M.T. Lee, T.L. Sun, W.C. Hung, H.W. Huang, Proc. Natl. Acad. Sci. U. S. A. 110 (2013) 14243–14248.
[47] E.H.L. Chen, C.H. Wang, Y.T. Liao, et al., Nat. Commun. 14 (2023) 5464.
[48] E.A. Masters, B.F. Ricciardi, K.L.M. Bentley, et al., Nat. Rev. Microbiol. 20 (2022) 385–400.
[49] Y. Wu, C. Raju, Z. Hou, et al., Biomaterials 273 (2021) 120794.